PERGAMON

International Journal of Multiphase Flow 28 (2002) 137–166

International Journal of Multiphase Flow

www.elsevier.com/locate/ijmulflow

Flow-aligned tensor models for suspension flows

Zhiwu Fang [a], Andrea A. Mammoli [a,*], John F. Brady [b], Marc S. Ingber [a], Lisa A. Mondy [c], Alan L. Graham [d]

[a] *Department of Mechanical Engineering, The University of New Mexico, Albuquerque, NM 87131, USA*
[b] *Department of Chemical Engineering, California Institute of Technology, Pasadena, CA 91125, USA*
[c] *Org. 9112, Sandia National Laboratories, Albuquerque, NM 87185, USA*
[d] *Department of Chemical Engineering, Texas Tech University, Lubbock, TX 79409, USA*

Received 8 May 2000; received in revised form 15 August 2001

Abstract

Models to describe the transport of particles in suspension flows have progressed considerably during the last decade. In one class of models, designated as suspension balance models, the stress in the particle phase is described by a constitutive equation, and particle transport is driven by gradients in this stress. In another class of models, designated as diffusive flux models, the motion of particles within the suspension is described through a diffusion equation based on shear rate and effective viscosity gradients. Original implementations of both classes of models lacked a complete description of the anisotropy of the particle interactions. Because of this, the prediction of particle concentration in torsional flows in parallel plate and cone-and-plate geometries did not match experimental data for either class of models. In this work, the normal stress differences for the suspension balance formulation are modeled using a frame-invariant flow-aligned tensor. By analogy, the diffusive flux model is reformulated using the same flow-aligned tensor, which allows separate scaling arguments for the magnitude of the diffusive flux to be implemented in the three principal directions of flow. Using these flow-aligned tensor formulations, the main shortcomings of the original models are eliminated in a unified manner. Steady-state and transient simulations are performed on various one-dimensional and two-dimensional flows for which experimental data are available, using finite-difference and finite-element schemes, respectively. The results obtained are in good agreement with experimental data for consistent sets of empirical constants, without the need for ad hoc additional terms.

1. Introduction

Particle migration in suspension flows is important in a variety of scientific and engineering applications including the transport of sediments, chromotography, composite materials

* Corresponding author.
E-mail address: mammoli@me.unm.edu (A.A. Mammoli).

0301-9322/02/$ - see front matter
PII: S0301-9322(01)00055-6

processing, sequestration processes in porous media, and secondary oil recovery techniques. Mesoscopic simulation, such as by Stokesian Dynamics and by boundary element methods (Brady and Bossis, 1985; Brady et al., 1988; Brady and Bossis, 1988; Brady, 1993; Chen and Doi, 1995; Ingber et al., 1994; Phan-Thien and Kim, 1994), can provide valuable insight into many-body interactions. Information about the microstructure of flowing suspensions such as anisotropic local structure and transition to a highly ordered state at high concentration may be obtained by dynamic simulation, as can the macroscopic rheological properties of suspensions. However, the number of particles explicitly modeled in these simulations is currently limited to on the order of several thousand using high-end computers because of the large CPU and memory requirements. From a practical point of view, a macroscopic constitutive equation is preferable, as it allows the modeling of realistic macroscopic problems which typically contain extremely large numbers of suspended particles. Several constitutive models have been put forth recently which basically fall into two categories. One category comprises models based on the conservation of mass and momentum for suspension components (Buyevich, 1995; Buyevich and Kapbsov, 1999; Jenkins and McTigue, 1990; Morris and Brady, 1998; Nott and Brady, 1994); the other category comprises models based on shear-induced particle migration and diffusion (Leighton and Acrivos, 1987a,b; Phillips et al., 1992).

The first category of models, collectively referred to in this paper as the "suspension balance" model, is based on statistical mechanics arguments. Balances are performed on mass and momentum for the particulate phase in a manner analogous to molecular systems. Although there is no explicit reference to the fluid in this model, the fluid does govern the nature of the interactions between particles. It is further assumed that the particles fluctuate with respect to their mean motion in a way analogous to molecular systems. These fluctuations are designated as the particle "temperature" and are introduced to provide a measure of non-locality in order to avoid the problems encountered by the model in regions where the local shear rate is zero. In the suspension balance model the conservation of momentum for the particle phase includes a constitutive equation for the particle stress. Nott and Brady (1994) derived an expression for the particle stress which included an isotropic pressure, a deviatoric shear stress and normal stress differences. Although the normal stress differences could be used to explain the absence of migration in the parallel plate geometry, the original paper by Nott and Brady did not postulate a form for this term. Subsequent papers by Brady and Morris (1997) and Morris and Boulay (1999) proposed models for the normal stress differences.

The second category of models, collectively referred to in this paper as the diffusive flux model, are based on scaling arguments proposed by Leighton and Acrivos (1987a,b) for two-body interactions. Particle migration and diffusion in the diffusive flux model is induced by a spatially varying inter-particle interaction frequency and effective viscosity. In particular, the shear-induced diffusivity scales linearly with the local shear rate. This model encounters difficulties in regions where the local shear rate approaches zero. For example, at the centerline of a Poiseuille flow a cusp in the concentration profile is predicted and the concentration goes to maximum packing. While this behavior may occur in the limit of $a \ll R$, where a is the particle radius and R is the radius of the pipe, it is aphysical for finite-sized particles. More severe limitations of the model occur in parallel plate and cone-and-plate geometries, however. In the parallel plate geometry, the diffusive flux model predicts inward particle migration, while in the cone-and-plate geometry the diffusive flux model predicts no migration at all. Both of these

predictions contradict experiments which show no detectable migration in the parallel plate geometry (Chow et al., 1994) and outward migration in the cone-and-plate geometry (Mondy and Altobelli, 1999; Chow et al., 1995). Krishnan et al. (1996) proposed an additional curvature-induced flux term for the diffusive flux model to overcome the deficiencies in the parallel plate and cone-and-plate geometries. Although this works for the parallel plate geometry, their radial flux term due to curvature is not frame invariant, and therefore cannot form the basis for a general constitutive theory.

In this paper, a normal stress difference model based on a flow-aligned directional tensor is implemented for the suspension balance model. The flow tensor's three principal directions are the three shear axes for general shearing flows (Bird et al., 1977). The current normal stress difference model is similar to the one proposed by Morris and Boulay (1999) except that it is argued here that none of the diagonal elements of the directional tensor are independent. Further, the so-called particle temperature (a measure of the particle fluctuating velocities) is retained in the current model for the normal stresses to introduce a measure of non-locality.

By analogy to the suspension balance model, a flow-aligned directional tensor is implemented in both flux terms in the diffusive flux model. The justification for this directional tensor is that the frequency of inter-particle interactions varies in the different flow directions. Hence, different diffusion rates can be modeled in the plane of shear and in the direction normal to it. This non-isotropic behavior corrects deficiencies for the diffusive flux model in parallel plate-and-cone-and-plate geometries.

The three principal directions for the flow-aligned tensors introduced for the modified suspension balance and diffusive flux models only exist, strictly speaking, for pure shearing flows. Nevertheless, the model is extended for general two-dimensional flows. In particular, the models are extended to the eccentric Couette problem and the piston-driven flow problem. Good agreement with experimental results is obtained for these two problems.

In Section 2 a detailed derivation of the extended suspension balance model is given. In Section 3 the modified diffusive flux model is presented. In Section 4 the equations at steady state for both models are simplified for one-dimensional flow, and numerical results are presented. In Section 5 transient velocity and particle concentration profiles are shown for circular Couette flow, eccentric journal bearing flow and piston-driven flow. The effects of bulk particle concentration and relative particle size on the time scale in a circular Couette device are investigated. Comparisons are made whenever possible with available experimental data.

2. The transient suspension balance model

2.1. Governing equations

The suspension balance model is derived by considering balance equations for both the suspension as a whole and for the particle phase (Nott and Brady, 1994). Conservation of mass and momentum for incompressible suspensions of neutrally buoyant particles can be obtained by averaging those quantities over all phases to obtain

$$\nabla \cdot \langle \mathbf{u} \rangle = 0, \tag{1}$$

$$\frac{\mathrm{D}\langle\rho\mathbf{u}\rangle}{\mathrm{D}t} = \langle\mathbf{b}\rangle + \nabla\cdot\langle\Sigma\rangle, \tag{2}$$

where

$$\frac{\mathrm{D}}{\mathrm{D}t} = \frac{\partial}{\partial t} + \langle\mathbf{u}\rangle\cdot\nabla \tag{3}$$

is the substantial derivative and $\langle\mathbf{u}\rangle$ is the volume averaged suspension velocity. The suspension stress $\langle\Sigma\rangle$ consists of contributions from both the fluid and particle phases (Batchelor, 1970)

$$\langle\Sigma\rangle = -\langle p\rangle_{\mathrm{f}}\mathbf{I} + 2\eta_{\mathrm{s}}\langle\mathbf{e}\rangle + \langle\Sigma\rangle_{\mathrm{p}}, \tag{4}$$

where $\langle p\rangle_{\mathrm{f}}$ is the averaged pressure in the fluid, η_{s} is the suspending fluid viscosity and $\langle\mathbf{e}\rangle$ is the bulk rate of strain tensor. The evolution of the particle concentration is governed by conservation of mass for the particle phase

$$\frac{\partial\phi}{\partial t} + \nabla\cdot\phi\langle\mathbf{u}\rangle_{\mathrm{p}} = 0, \tag{5}$$

where $\langle\mathbf{u}\rangle_{\mathrm{p}}$ is the particle-phase average velocity. The difference between the averaged suspension velocity $\langle\mathbf{u}\rangle$ and the averaged particle velocity $\langle\mathbf{u}\rangle_{\mathrm{p}}$ is related to the drag force exerted on the particles $\langle\mathbf{F}\rangle_{\mathrm{p}}$. At low particle Reynolds number this relation is linear

$$\langle\mathbf{u}\rangle - \langle\mathbf{u}\rangle_{\mathrm{p}} = M(\eta_{\mathrm{s}}, a, \phi)\langle\mathbf{F}\rangle_{\mathrm{p}}, \tag{6}$$

where $M(\eta_{\mathrm{s}}, a, \phi)$ is a coefficient that accounts for the hindered mobility of an average particle caused by the surrounding particles, with the assumption that the mobility is isotropic.

Combining Eq. (5) with Eq. (6), a particle conservation equation can be written as

$$\frac{\partial\phi}{\partial t} + \langle\mathbf{u}\rangle\cdot\nabla\phi = \nabla\cdot\mathbf{N}, \tag{7}$$

where the particle flux (relative to the suspension average velocity) is given by

$$\mathbf{N} = \phi M(\eta_{\mathrm{s}}, a, \phi)\langle\mathbf{F}\rangle_{\mathrm{p}}. \tag{8}$$

The average particle drag force can be obtained by considering the momentum balance for the particle phase

$$\rho_{\mathrm{p}}\phi\frac{\mathrm{D}_{\mathrm{p}}\langle\mathbf{u}\rangle_{\mathrm{p}}}{\mathrm{D}t} = \langle\mathbf{b}\rangle_{\mathrm{p}} + \langle\mathbf{F}\rangle_{\mathrm{p}} + \nabla\cdot\langle\Sigma\rangle_{\mathrm{p}}, \tag{9}$$

where the substantial derivative is now that following the average particle motion, $\langle\Sigma\rangle_{\mathrm{p}}$ is the particle stress, and $\langle\mathbf{b}\rangle_{\mathrm{p}}$ is the particle body force, which is zero for the neutrally buoyant particles considered here.

In many suspension flows the Reynolds number based on the particle motion is negligibly small, typically of order 10^{-4}. If the motion on the macroscale – the scale of the device geometry – is also at low Reynolds number, which is true for the cases considered here, then the inertial term on the left-hand side of (9) can be neglected and the drag force can be solved for explicitly

$$\langle\mathbf{F}\rangle_{\mathrm{p}} = -\langle\mathbf{b}\rangle_{\mathrm{p}} - \nabla\cdot\langle\Sigma\rangle_{\mathrm{p}}, \tag{10}$$

which shows that the particle flux $\mathbf{N}$ is driven by body forces ($\langle\mathbf{b}\rangle_{\mathrm{p}}$) and stress gradients ($\nabla\cdot\langle\Sigma\rangle_{\mathrm{p}}$).

Several approaches have been taken to model the particle-phase stress. In this work we follow the approach of Nott and Brady (1994) whereby the averaged particle-phase stress is comprised of the particle pressure, a deviatoric shear stress, and normal-stress differences. At small particle-scale Reynolds number, the constitutive equation for the particle-phase stress is given by

$$\langle \Sigma \rangle_{\mathrm{p}} = -\Pi \mathbf{I} + 2\eta_{\mathrm{s}}\eta_{\mathrm{p}}(\phi)\langle \mathbf{e} \rangle + \eta_{\mathrm{s}}\langle \chi \rangle, \tag{11}$$

where Π is the particle pressure, $\eta_{\mathrm{p}}(\phi)$ is the particle-phase relative viscosity and χ is the normal-stress difference. Nott and Brady (1994) only considered rectilinear flows where normal stress differences are not important. Here, the model is extended to include the effect of normal stress differences, as they play an important role in curvilinear flows.

To model the normal stresses, we follow the work of Brady and Morris (1997), where it was shown that normal stresses linear in the shear rate are to be expected in concentrated suspensions due to any one of residual Brownian motion (finite Peclet numbers), short-range non-hydrodynamic interparticle forces or surface roughness. Since the normal stress differences have the same microstructural origin as the particle-phase pressure, and therefore have the same scaling with shear rate and volume fraction, the particle stress can be written as

$$\langle \Sigma \rangle_{\mathrm{p}} = -\Pi \mathbf{Z} + 2\eta_{\mathrm{s}}\eta_{\mathrm{p}}(\phi)\langle \mathbf{e} \rangle, \tag{12}$$

where the tensor $\mathbf{Z}$ depends on the flow type and gives the normal stress components. The 'pressure' Π is now a function of the volume fraction and shear rate and is given by

$$\Pi = \eta_{\mathrm{s}}\dot{\gamma}\bar{p}(\phi), \tag{13}$$

where $\dot{\gamma} = (\langle \mathbf{e} \rangle \cdot \langle \mathbf{e} \rangle)^{1/2}$ and $\bar{p}(\phi)$ is a monotonically increasing function of ϕ.

The particle-phase viscosity is related to the relative viscosity of the suspension (the viscosity of the suspension measured in a rheometer normalized by the solvent viscosity) by

$$\eta_{\mathrm{r}} = 1 + \eta_{\mathrm{p}}(\phi), \tag{14}$$

and the relative viscosity is modeled from the correlation of Krieger

$$\eta_{\mathrm{r}} = \left(1 - \frac{\phi}{\phi_{\mathrm{m}}}\right)^{-1.82} \tag{15}$$

in which ϕ_{m} is the maximum solid volume fraction for which the suspension exhibits fluid behavior. The value of ϕ_{m} depends on several factors as discussed by Subia et al. (1998). In this research, ϕ_{m} is chosen to be 0.68 in all calculations.

The normal stress tensor $\mathbf{Z}$ depends on the flow type, for example simple shear or extensional flow, and can be determined from a microstructural model, such as the one derived by Brady and Morris (1997). However, a simple general expression can be developed as Morris and Boulay (1999) have done, by expressing $\mathbf{Z}$ in a local flow-aligned principal direction system with unit vectors $\boldsymbol{\delta}_1$, $\boldsymbol{\delta}_2$, and $\boldsymbol{\delta}_3$, which form a right-handed coordinate set, defined as follows: $\boldsymbol{\delta}_3$ is in the direction of the eigenvector of the rate of strain tensor $\langle \mathbf{e} \rangle$ associated with the eigenvalue of minimum magnitude (zero in the case of a shear flow); $\boldsymbol{\delta}_1$ and $\boldsymbol{\delta}_2$ are the shear axes, with $\boldsymbol{\delta}_1$ chosen between the shear axes such that $\boldsymbol{\delta}_1 \cdot \nabla \hat{\mathbf{v}}$ is minimized, where $\hat{\mathbf{v}}$ is a modified velocity field obtained by subtracting any overall rigid body rotation from the original velocity field. Note that in the

cases considered here, the direction of $\boldsymbol{\delta}_1$ coincides with the direction of velocity. This will not be the case for generic complex flows. Furthermore, because of the isotropy of the model in the shear plane, this distinction is not necessary.

With this choice of axes, the plane of shear is defined by the unit vectors $\boldsymbol{\delta}_1$ and $\boldsymbol{\delta}_2$. Also, because the axes are based on the rate of strain tensor, they are frame-independent. In general, the principal directions of the flow are not necessarily the principal directions of the normal stress tensor; however, the Stokesian Dynamics simulations by Sami (1996) of Brownian hard spheres show that both the shear and normal stresses for planar extensional flow can be mapped one-to-one to those for simple shear flow for all volume fractions and shear rates (Peclet numbers). Thus, it should be a good approximation to take $\mathbf{Z}$ as diagonal in the flow-aligned directions defined above

$$\mathbf{Z} = \begin{pmatrix} \lambda_1 & 0 & 0 \\ 0 & \lambda_2 & 0 \\ 0 & 0 & \lambda_3 \end{pmatrix}, \tag{16}$$

where the values of λ_i need to be determined by experiment, simulation or from microstructural modeling. The flow-aligned tensor gives the following forms for the normal stress differences and particle pressure:

$$\sigma_{11} - \sigma_{22} = -\Pi(\lambda_1 - \lambda_2), \tag{17}$$

$$\sigma_{22} - \sigma_{33} = -\Pi(\lambda_2 - \lambda_3) \tag{18}$$

and

$$\Pi = \Pi\left(\frac{\lambda_1 + \lambda_2 + \lambda_3}{3}\right). \tag{19}$$

Since the particle pressure has been defined as Π, it is required that $\lambda_1 + \lambda_2 + \lambda_3 = 3$. As there are virtually no experiments measuring normal stresses in suspension flows (see the recent work of Zarraga et al. (2000) for a notable exception), modeling will be used to estimate the relative magnitudes of λ_1, λ_2 and λ_3 indirectly from experimental measurements of particle concentration profiles.

Brady and Morris (1997) derived a microstructural model relating suspension stress to the flow-induced microstructure. They show that the dominant contribution to the stress comes from a boundary layer at particle-particle contact and obtain an appropriate solution for the structure and stress that gives a zero first normal stress difference and a negative second normal stress difference in simple shear flow. The specific predictions in terms of λ are

$$\lambda_1 = \lambda_2 = 2\lambda_3. \tag{20}$$

They also offer a scaling expression for the function $\bar{p}(\phi)$

$$\bar{p}(\phi) \sim \phi^2\left(1 - \frac{\phi}{\phi_{\max}}\right)^{-2}. \tag{21}$$

The available Stokesian Dynamics simulation results by Phung et al. (1996), Yurkovetsky and Brady (1996) and Foss and Brady (1999) and the experiments by Zarraga et al. (2000) show that $N_2 < 0$ and that N_1, while not zero as the radial-balance approximation of Brady

and Morris (1997) suggests, is negative and smaller in magnitude than N_2. The volume fraction scaling of $\bar{p}(\phi)$ suggested by Brady and Morris (1997) is in reasonably good agreement with the simulation results of Yurkovetsky and Brady (1996) and Foss and Brady (1999).

Morris and Boulay (1999) chose $\lambda_2 = 0.8\lambda_1$, resulting in a small negative N_1. Although N_1 is probably not zero for an actual suspension, the simple relationship given by Eq. (20) will be used in this work. As will be shown below, this choice predicts no migration in torsional flow between parallel plates and outward migration in cone-and-plate flow, as has been observed experimentally (Chapman, 1990; Chow et al., 1994, 1995).

In a cylindrical coordinate system (r, θ, z), the flow-aligned tensor $\mathbf{Z}$ for torsional flow between parallel plates is given by

$$\mathbf{Z} = \begin{pmatrix} \lambda_3 & 0 & 0 \\ 0 & \lambda_1 & 0 \\ 0 & 0 & \lambda_2 \end{pmatrix}, \tag{22}$$

while the rate of strain tensor $\langle \mathbf{e} \rangle$ is

$$\langle \mathbf{e} \rangle = \begin{pmatrix} 0 & 0 & 0 \\ 0 & 0 & \dot{\gamma}_{\theta z} \\ 0 & \dot{\gamma}_{\theta z} & 0 \end{pmatrix}. \tag{23}$$

The shear rate is linear in r: $\dot{\gamma}_{\theta z} = (\omega/H)r$, where H and ω are the gap between the plates and their relative rotational velocities, respectively. Hence, the flux components, $\mathbf{N} = \nabla \cdot \langle \Sigma \rangle_{\mathrm{p}}$, are given by

$$\begin{aligned} N_{\mathrm{r}} &= \frac{1}{r}\frac{\partial}{\partial r}\left(r\langle \Sigma \rangle_{\mathrm{p}}^{rr}\right) + \frac{1}{r}\frac{\partial}{\partial \theta}\left(\langle \Sigma \rangle_{\mathrm{p}}^{\theta r}\right) + \frac{\partial}{\partial z}\langle \Sigma \rangle_{\mathrm{p}}^{zr} - \frac{\langle \Sigma \rangle_{\mathrm{p}}^{\theta\theta}}{r} \\ &= \frac{\partial}{\partial r}\langle \Sigma \rangle_{\mathrm{p}}^{rr} + \frac{\langle \Sigma \rangle_{\mathrm{p}}^{rr} - \langle \Sigma \rangle_{\mathrm{p}}^{\theta\theta}}{r} = -\lambda_3 \frac{\partial}{\partial r}\Pi + \frac{-\lambda_3 + \lambda_1}{r}\Pi. \end{aligned} \tag{24}$$

Because it is assumed that no there is no θ or z dependence,

$$N_\theta = 0, \tag{25}$$

$$N_z = 0. \tag{26}$$

At steady state, particle conservation, Eq. (7), implies that $\nabla \cdot \mathbf{N} = 0$, and hence N_{r} must be constant. Further, since at the outer boundary $N_{\mathrm{r}} = 0$, N_{r} must be zero throughout the flow domain. As a result,

$$\lambda_3 \frac{\partial \Pi}{\partial r} = \frac{(\lambda_1 - \lambda_3)\Pi}{r}, \tag{27}$$

with solution

$$\Pi = Ar^{(\lambda_1 - \lambda_3)/\lambda_3}, \tag{28}$$

where A is a constant. Since $\dot{\gamma}_{\theta z} = (\omega/H)r$, we have

$$\bar{p}(\phi) = \frac{AH}{\omega} r^{(\lambda_1 - 2\lambda_3)/\lambda_3}. \tag{29}$$

With the choice of $\lambda_1 = 2\lambda_3$, $\bar{p}(\phi)$ becomes constant, resulting in no migration in torsional flow between parallel plates, in accordance with the experimentally observed lack of migration, and with the prediction of Brady and Morris (1997).

In the cone-and-plate geometry, the flow-aligned tensor, $\mathbf{Z}$, in spherical coordinates (r,ψ,θ) (where ψ is the azimuthal angle and θ is the polar angle) becomes

$$\mathbf{Z} = \begin{pmatrix} \lambda_3 & 0 & 0 \\ 0 & \lambda_2 & 0 \\ 0 & 0 & \lambda_1 \end{pmatrix}. \tag{30}$$

The bulk rate of strain tensor $\langle \mathbf{e} \rangle$ for the resulting flow can be written as

$$\langle \mathbf{e} \rangle = \begin{pmatrix} 0 & 0 & 0 \\ 0 & 0 & \dot{\gamma}_{\theta\psi} \\ 0 & \dot{\gamma}_{\theta\psi} & 0 \end{pmatrix}, \tag{31}$$

in which the constant $\dot{\gamma}_{\theta\psi}$ is again the only non-zero shear component.

The flux component in the ψ-direction is given by

$$N_\psi = \frac{1}{r^3}\frac{\partial}{\partial r}\left(r^3 \langle \Sigma \rangle_{\mathrm{p}}^{r\psi}\right) + \frac{1}{r\sin\psi}\frac{\partial}{\partial \psi}\left(\langle \Sigma \rangle_{\mathrm{p}}^{\psi\psi}\sin\psi\right) + \frac{1}{r\sin\psi}\frac{\partial}{\partial \theta}\langle \Sigma \rangle_{\mathrm{p}}^{\theta\psi} + \frac{\langle \Sigma \rangle_{\mathrm{p}}^{\psi r} - \langle \Sigma \rangle_{\mathrm{p}}^{r\psi} - \langle \Sigma \rangle_{\mathrm{p}}^{\theta\theta}\cot\psi}{r}. \tag{32}$$

At steady state, because the suspension velocity is in the polar direction, this azimuthal flux must be zero. Because of symmetry considerations, it seems reasonable to assume that $\partial\phi/\partial\psi = 0$. It may also be argued that a thin shell of fluid at a given radial position should behave as a homogeneous shear flow, which leads to the same conclusion. However, neither of these arguments provides a rigorous proof that the concentration in the ψ direction should be uniform. Experimental or numerical evidence that either supports or disproves this assumption would be a useful addition to the body of evidence upon which these models are based. Setting $N_\psi = 0$ and substituting Eqs. (30) and (31) into Eq. (32) yields

$$\frac{1}{r\sin\psi}\frac{\partial}{\partial \psi}\left(\langle \Sigma \rangle_{\mathrm{p}}^{\psi\psi}\sin\psi\right) - \frac{\langle \Sigma \rangle_{\mathrm{p}}^{\theta\theta}}{r}\cot\psi = 0, \tag{33}$$

or

$$\frac{1}{r}\frac{\partial}{\partial \psi}(-\lambda_2 \Pi) + \frac{\cot\psi}{r}(-\lambda_2 \Pi) - \frac{\cot\theta}{r}(-\lambda_1 \Pi) = 0. \tag{34}$$

The solution to Eq. (34) is given by

$$\Pi = B(r)(\sin\psi)^{(\lambda_2-\lambda_1)/\lambda_1}. \tag{35}$$

Because of the assumption made regarding the uniformity of ϕ in the ψ direction, the particle pressure cannot depend on the azimuthal angle ψ at steady state. Hence, from Eq. (35), $\lambda_1 = \lambda_2$. This is also in accordance with the model predictions of Brady and Morris (1997).

With this specification of the normal stresses, the model is now complete and can be used to predict velocity and concentration profiles in any flow geometry. The model as posed does have one deficit, namely that, where the shear rate vanishes, the particle pressure induces a concentration that approaches maximum packing. As discussed by Nott and Brady (1994), one way to overcome this difficulty is to introduce the suspension temperature to render the model non-local. Following Nott and Brady (1994), the particle pressure is now written as

$$\Pi = a^{-1}\eta_s p(\phi) T^{1/2}, \tag{36}$$

where

$$T = \langle \mathbf{u}' \cdot \mathbf{u}' \rangle_p \tag{37}$$

is the particle temperature, and

$$p(\phi) = k_\phi \phi^{1/2} \eta_p^{\xi} \tag{38}$$

is a monotonically increasing function of the particle concentration. The value of the exponent ξ will be discussed in Section 4.

An equation for the temperature can be derived from a mechanical energy balance on the particle phase

$$\rho_p \phi C(\phi) \frac{D_p T}{Dt} = \langle \Sigma \rangle_p : \nabla \langle \mathbf{u} \rangle_p + \eta_s a^{-2} \beta(\phi) T^{1/2} (u_s^2)^{1/2} - \eta_s a^{-2} \alpha(\phi) T - \nabla \cdot \mathbf{q}, \tag{39}$$

where u_s is the slip velocity between the particle and the suspension phases ($u_s^2 = (\langle \mathbf{u} \rangle_p - \langle \mathbf{u} \rangle) \cdot (\langle \mathbf{u} \rangle_p - \langle \mathbf{u} \rangle)$), α, β and C are non-dimensional functions of ϕ and $\mathbf{q}$ is the 'heat flux' vector.

For the high Peclet number, non-inertial suspensions considered here, the relaxation of fluctuations occurs very quickly (with time scales of $\dot{\gamma}^{-1}Pe^{-1}$ or $\dot{\gamma}^{-1}St$, respectively, where the Stokes number $St = \rho_p \dot{\gamma} a^2/\eta_s$) and any 'heat capacity' effects can be neglected.

In simple homogeneous shearing motion there is no phase slip, and Eq. (39) gives the particle temperature as

$$T = (\dot{\gamma} a)^2 \frac{\eta_p(\phi)}{\alpha(\phi)}, \tag{40}$$

showing that the function $\alpha(\phi)$ determines the fluctuation velocity for shearing motion. In a like manner, in a homogeneous sedimentation experiment there is no shearing motion but there is phase slip, and $\beta(\phi)$ then sets the fluctuating velocity in terms of the external body force which drives the phase slip

$$T = \left(\frac{\beta}{\alpha}\right)^2 u_s^2. \tag{41}$$

In shear dominated flows the phase slip is small ($O(a/H)^2$), and, as this work focuses on shearing flows, the energy associated with the phase slip will be neglected. Finally, the heat flux vector $\mathbf{q}$ is modeled by a Fourier-type law

$$\mathbf{q} \equiv -\langle \Sigma_p' \cdot \mathbf{u}_p' \rangle = -\eta_s \kappa(\phi) \nabla T, \tag{42}$$

where $\kappa(\phi)$ is the non-dimensional conductivity.

In homogeneous shear flow it is entirely equivalent to take the pressure as proportional to $\dot{\gamma}$ as in Eq. (11) or proportional to $T^{1/2}$ as in Eq. (36), that is,

$$p(\phi)\left(\frac{\eta_p}{\alpha}\right)^{1/2} = \bar{p}(\phi). \tag{43}$$

In inhomogeneous flows however, due to the conduction of fluctuational motion caused by the finite size of the particles, the temperature is not necessarily zero when the macroscopic shear rate vanishes. This finite particle size effect renders the model non-local and removes the feature that the concentration approaches maximum packing where the shear rate vanishes. There are other ways to render the model non-local, and a scalar temperature is probably an oversimplification (especially in the vicinity of walls), but it is one of the simplest invariant formulations possible.

The form of the phenomenological coefficients now needs to be specified. A suitable form for particle mobility M can be determined empirically or by particle-level numerical simulation. The simplest experimental approach is to relate M to the hindered settling function

$$M(\eta_s, a, \phi) = \frac{2}{9}\frac{a^2 h(\phi)}{\phi \eta_s}, \tag{44}$$

where, following Kapoor and Acrivos (1995) the hindered settling function $h(\phi)$ is given by

$$h(\phi) = \frac{1-\phi}{\eta_r(\phi)}, \tag{45}$$

and the relative viscosity is given by Eq. (15).

Following Nott and Brady (1994), the functions $\alpha(\phi)$ and $\kappa(\phi)$ are chosen to be

$$\alpha(\phi) = \frac{k_\alpha}{\phi}\eta_p(\phi), \tag{46}$$

and

$$\kappa(\phi) = k_\kappa \eta_p(\phi). \tag{47}$$

In all calculations, the original values for k_α and k_κ proposed by Nott and Brady, 0.19 and 0.17, respectively, are adopted. An additional constant, k_ϕ, is required to account for the irreversibility of interparticle interactions in the particle pressure. This constant appears in Eq. (38); the pressure Π is directly proportional to k_ϕ, and consequently, if $k_\phi = 0$, as would be the case with perfectly reversible interactions, the particle pressure would also be zero. In this work, the value of k_ϕ can be inferred from transient experimental results, as shown later.

No-slip velocity boundary conditions for the suspension average velocity field are assumed; there is little modeling or experimentation directed towards the determination of the proper boundary conditions and this simple choice is reasonable. The normal particle flux at the walls is zero, and the bulk concentration (or flux, as appropriate) is kept constant. In their calculations, Nott and Brady (1994) specified $T = 0$ on solid walls. However, this would allow the wall concentration to reach maximum packing. In fact, the particle temperature is not necessarily zero on the solid wall, because particles in the vicinity of solid walls are still able to fluctuate along the direction tangential to or away from solid walls. In all simulations using the suspension balance

model in this paper, the wall temperature is given by the empirical equation proposed by Morris and Brady (1998), namely

$$T = 2\frac{a^2\phi}{k_\alpha}\langle \mathbf{e}\rangle : \langle \mathbf{e}\rangle. \tag{48}$$

3. Modified diffusive-flux model

Although we have already derived an expression for the particle flux from the suspension balance model, it is interesting to try to extend the original diffusive flux model to incorporate the effects of normal stress differences. In the absence of Brownian motion and assuming that sedimentation is not present because of neutral buoyancy, the diffusive particle flux as proposed by Leighton and Acrivos (1987b) can be modeled as

$$\mathbf{N} = \mathbf{N}_\eta + \mathbf{N}_c, \tag{49}$$

where $\mathbf{N}_\eta$ is the flux contribution due to spatial variations in viscosity and $\mathbf{N}_c$ is the flux contribution due to hydrodynamic particle interactions. Using the scaling arguments of Leighton and Acrivos (1987b), these flux terms, as originally proposed by Phillips et al. (1992) are given by

$$\mathbf{N}_c = -K_c a^2 \phi \nabla(\dot{\gamma}\phi) \tag{50}$$

and

$$\mathbf{N}_\eta = -K_\eta a^2 \phi(\dot{\gamma}\phi)\nabla \ln \eta, \tag{51}$$

where a is the characteristic particle size, $\dot{\gamma}$ is a measure of the generalized shear rate given by $\dot{\gamma} = 2(\langle \mathbf{e}\rangle : \langle \mathbf{e}\rangle)^{1/2}$, $\eta(\phi)$ is the viscosity of the suspension, and K_c and K_η are empirically determined coefficients. A conservation equation for the solid particles can then be written as

$$\frac{\mathrm{D}\phi}{\mathrm{D}t} = -\nabla \cdot (\mathbf{N}_c + \mathbf{N}_\eta). \tag{52}$$

This model is analogous to a statistical gas model in that a test particle will perform a random walk from regions of high frequency of interactions to regions of low frequency of interactions. The $\mathbf{N}_c$ flux term indicates that gradients in interaction frequency are determined by both gradients in shear rate and gradients in concentration. The $\mathbf{N}_\eta$ flux term indicates that the magnitude of particle flux is also governed by the relative viscosity of the suspension which affects the mobility of the particles.

Although the original diffusive flux model as outlined above was successful in modeling several benchmark problems (see, e.g., Subia et al., 1998), it did exhibit problems for both the parallel plate and cone-and-plate geometries, as discussed in Section 1. One possible reason for these deficiencies is that the particle interaction-induced flux term, $\mathbf{N}_c$, is isotropic. Even though the frequency of interaction scales as $\dot{\gamma}\phi$, the random walk of the test particle is more likely to occur in the plane of shear rather than in the direction normal to the plane of shear. This non-isotropic behavior is not modeled in the original diffusive flux model.

To resolve the non-isotropic behavior of the particle flux at a point, the diffusive flux model is simply modified by using the flow-aligned tensor $\mathbf{Z}$ as:

$$\mathbf{N}_c = -K_c a^2 \phi \nabla \cdot (\dot{\gamma}\phi \mathbf{Z}), \tag{53}$$

and

$$\mathbf{N}_\eta = -K_\eta a^2 \phi (\dot{\gamma}\phi \mathbf{Z}) \cdot \nabla \ln \eta. \tag{54}$$

The original isotropic formulation can be recovered by choosing $\mathbf{Z}$ to be the identity tensor. To obtain a more general anisotropic model however, values for λ_i need to be correlated for the different flux rates in the direction of the shear axes. Clearly, for the modified diffusive flux model to be useful λ_i should be independent of the local flow field. As was the case for the suspension balance model, λ_i can be chosen by considering experimental results from selected flow geometries.

The values of λ_i in the modified diffusive flux model are not necessarily the same as those in the modified suspension balance model because of the different physical quantities represented by the flow-aligned tensor $\mathbf{Z}$ in the two models. Nevertheless, it will be shown that the same set of relations are obtained between the λ's for the two models. Indeed Brady and Morris (1997) showed that there is a direct relation between stress and diffusion so that it is to be expected that the two models should have the same values of λ_i.

In the parallel plate geometry the flow-aligned tensor for the resulting torsional flow in cylindrical coordinates (r, θ, z) transforms to the tensor shown in Eq. (22). The flux components in the r, θ, and z directions are given by

$$\begin{aligned} N_r &= -K_c a^2 \phi \left[\frac{1}{r} \frac{\partial}{\partial r} (\dot{\gamma}\phi Z_{rr}) - \frac{\dot{\gamma}\phi Z_{\theta\theta}}{r} \right] - K_\eta a^2 \dot{\gamma} \phi^2 \frac{\partial \ln \eta}{\partial r} Z_{rr} \\ &= -K_c a^2 \phi^2 \left(\frac{\partial \dot{\gamma}}{\partial r} \lambda_3 + \frac{\lambda_3 - \lambda_2}{r} \dot{\gamma} \right) - K_c a^2 \phi \dot{\gamma} \left(1 + \phi \frac{\mathrm{d} \ln \eta}{\mathrm{d}\phi} \frac{K_\eta}{K_c} \right) \lambda_3 \frac{\partial \phi}{\partial r} \\ &= -K_c a^2 \phi^2 (2\lambda_3 - \lambda_2) - K_c a^2 \phi \dot{\gamma} \left(1 + \phi \frac{\mathrm{d} \ln \eta}{\mathrm{d}\phi} \frac{K_\eta}{K_c} \right) \lambda_3 \frac{\partial \phi}{\partial r}, \end{aligned} \tag{55}$$

$$N_\theta = 0, \tag{56}$$

and

$$N_z = 0, \tag{57}$$

respectively. As in the case of the suspension balance model, it is argued that at steady state the divergence of the flux must be zero, which implies $N_r = 0$. Experimental evidence (Chapman, 1990; Chow et al., 1994), indicates that either no or, at best, weak migration exists in the parallel plate geometry. In particular, at steady state the concentration profile in this geometry is essentially uniform, and it follows that $\partial\phi/\partial r = 0$, and hence from (55), $\lambda_3 = \frac{1}{2}\lambda_2$.

In the cone-and-plate geometry using the spherical coordinate system (r, ψ, θ), the flow-aligned tensor $\mathbf{Z}$ is again transformed as shown in (30). The diffusive flux component in the ψ-direction is given by

$$N_\psi = -K_c a^2 \phi \left[\frac{1}{r \sin\psi} \frac{\partial}{\partial \psi} \left(\dot{\gamma} \phi Z_{\psi\psi} \sin\psi \right) - \frac{\dot{\gamma} \phi Z_{\theta\theta}}{r} \cot\psi \right] - K_\eta a^2 \dot{\gamma} \phi^2 \frac{\partial \ln \eta}{\partial r} Z_{rr}$$

$$= -K_c a^2 \dot{\gamma} \phi \left[(\lambda_2 - \lambda_1) \frac{\phi}{r} \cot\psi \right] - a^2 \dot{\gamma} \phi \left(K_c + K_\eta \phi \frac{\mathrm{d} \ln \eta}{\mathrm{d}\phi} \right) \frac{1}{r} \frac{\partial \phi}{\partial \psi} \lambda_2. \tag{58}$$

As discussed for the suspension balance model, this flux component is assumed to be zero at steady state. Hence, from (58), $\lambda_2 = \lambda_1$. By setting $N_r = 0$, an analytic solution for $\phi(r)$ can be obtained for the cone-and-plate geometry as discussed in Section 4.

Having $\lambda_1 = \lambda_2 = 2\lambda_3$ indicates that hydrodynamic interactions between particles and subsequent random walk are more likely to occur in the directions of flow and velocity gradient than in the vorticity direction, a result predicted for diffusion by Brady and Morris (1997).

Finally, to complete the diffusive flux model, a constitutive equation is needed for the suspension stress. Here, a term must be added to the generalized Newtonian constitutive equation for the stress in order to reflect the presence of normal stress differences. The constitutive equation now becomes

$$\langle \Sigma \rangle = -\langle p \rangle_f \mathbf{I} + 2\eta_s \eta_r(\phi) \langle \mathbf{e} \rangle - \eta_s \eta_p(\phi) \dot{\gamma} \mathbf{Z}. \tag{59}$$

4. Steady-state benchmark results

Four benchmark problems are considered in this section including flow in a Couette device, pressure-driven pipe flow, pressure-driven flow between parallel plates, and torsional flow in a cone-and-plate viscometer. A fifth benchmark should also be mentioned, namely, torsional flow between parallel plates. However, by construction, both the modified diffusive flux model and modified suspension balance model will predict a homogeneous concentration profile at steady state, and hence, the velocity field is the same as given by a homogeneous Newtonian fluid. This is a significant improvement for the diffusive flux model which originally predicted inward migration for torsional flow between parallel plates.

4.1. Couette flow

A considerable quantity of experimental data have become available for circular Couette flow (Abbott et al., 1991; Phillips et al., 1992; Tetlow et al., 1998), and the initial comparisons are performed for this geometry. The momentum equations for both the modified diffusive flux model and the modified suspension balance model are given by

$$\frac{\mathrm{d}}{\mathrm{d}r} \left[r^3 \eta_r \frac{\partial}{\partial r} \left(\frac{u_\theta}{r} \right) \right] = 0, \tag{60}$$

where the angle brackets denoting the suspension average have been dropped. All lengths have been non-dimensionalized by the separation between the cylinders, H, and the velocities by the rotating cylinder velocity, $U = \Omega R$.

The concentration equations for the modified suspension balance model and the modified diffusive flux model take the following forms, respectively:

$$\frac{\mathrm{d}}{\mathrm{d}r}(p(\phi)\sqrt{T}) = 0, \tag{61}$$

and

$$-K_c a^2 \phi \frac{\mathrm{d}(\dot{\gamma}\phi)}{\mathrm{d}r} - K_\eta a^2 \dot{\gamma}\phi^2 \frac{\mathrm{d}\ln\eta}{\mathrm{d}\phi}\frac{\mathrm{d}\phi}{\mathrm{d}r} = 0. \tag{62}$$

The particle temperature equation for the suspension balance model is given by

$$\epsilon^2 \frac{1}{r}\frac{\partial}{\partial r}\left[r\kappa(\phi)\frac{\partial T}{\partial r}\right] - \alpha(\phi)T + \eta_p\left[r\frac{\partial}{\partial r}\left(\frac{u_\theta}{r}\right)\right]^2 = 0, \tag{63}$$

where the relative particle size, ϵ, for the Couette geometry is defined by $\epsilon = a/R_o$, where R_o is the outer cylinder radius and a the particle radius.

An analytic solution is possible in this case for the modified diffusive flux model and is exactly the same as in the original model

$$\left(\frac{r}{r_w}\right)^2 = \frac{\phi}{\phi_w}\left(\frac{\phi_m - \phi_w}{\phi_m - \phi}\right)^{\xi\left(K_\eta/K_c - 1\right)}. \tag{64}$$

The equations for the modified suspension balance model are solved using a finite difference method. A Newton iteration is used to obtain the temperature and concentration profiles. After the concentration profile is known, the velocity profile is easily obtained from Eq. (60) and the procedure repeated until convergence is obtained. The power index ξ which appears in the model for the function p Eq. (38) is determined by comparing numerical results with experimental data. The effect of ξ on the predicted concentration profiles is shown in Fig. 1(a).

From inspection, $\xi = 1.5$ appears to provide the best fit to the experimental data. All numerical results presented hereafter reflect this choice of the power index. It should be noted that, at low ϕ,

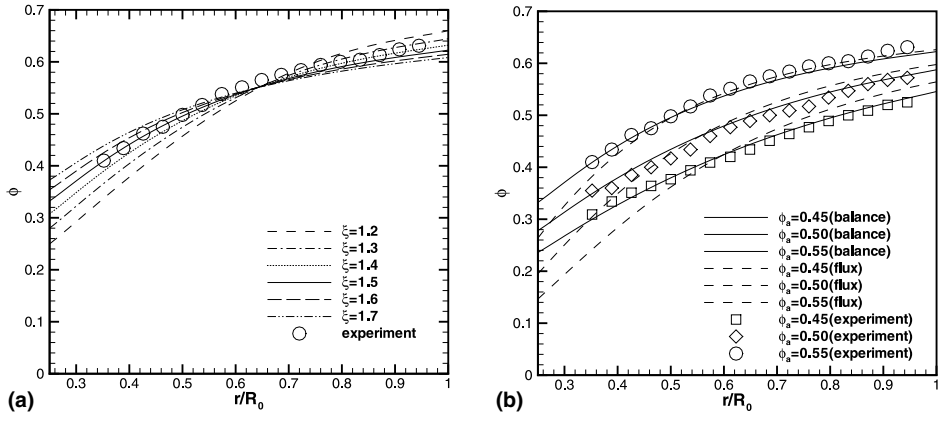

Fig. 1. (a) The effect of the power index, ξ, on the calculated concentration profile for bulk concentration $\phi_a = 0.55$ and $\epsilon = 0.02836$. Experimental data are from Abbott et al. (1991). (b) Comparison of model predictions with experimental concentration profiles, $\epsilon = 0.02836$. Solid lines are predictions by the suspension balance model and dashed lines are predictions by the diffusive flux model.

the power index should become 1.0, to yield the correct $O(\phi^2)$ scaling for the pressure. However, at higher values of ϕ, it is plausible that higher power index values apply.

A comparison of the predicted steady-state profiles obtained using the modified suspension balance and diffusive flux models with experimental concentration profiles is shown in Fig. 1(b) for bulk volume concentrations, ϕ_a, of 45%, 50% and 55%.

The suspension balance model predictions match the experimental data better over the range of concentrations considered. However, as discussed by Tetlow et al. (1998), better predictions can be made with the diffusive flux models if the diffusivity coefficients K_c and K_η are chosen as functions of the local volume concentrations. This was not done in the current calculation but rather the constant values chosen by Phillips et al. (1992) were used, namely, $K_c = 0.41$ and $K_\eta = 0.62$. Indeed, comparison of the expression for the particle flux from the suspension balance model with that from the diffusive flux model shows that ϕ-dependent K_c and K_η can be chosen to make the two models identical in the limit of small ϵ.

The diffusive flux model predicts no dependence of the relative particle size, ϵ, on the steady-state concentration profile. The suspension balance model, on the other hand, does predict a dependence of the relative particle size on steady-state characteristics as shown in Fig. 2 for the concentration profile. However, as seen in Fig. 2 for $\epsilon < 0.05$ there is very little influence of ϵ on the concentration profile, which is confirmed by the experiments performed by Tetlow et al. (1998). The effect of ϵ on the concentration profile is only seen at values of ϵ larger than 0.1. For such values, these models may not be applicable because the continuum approximation may break down.

4.2. Circular Poiseuille flow

The second benchmark problem is pressure-driven flow in a circular pipe. For fully developed steady-state flow, the momentum equation for both models is given by

$$\frac{1}{r}\frac{\mathrm{d}}{\mathrm{d}r}\left(r\eta_r\frac{\mathrm{d}u_z}{\mathrm{d}r}\right) = -\frac{\mathrm{d}p_s}{\mathrm{d}z}, \tag{65}$$

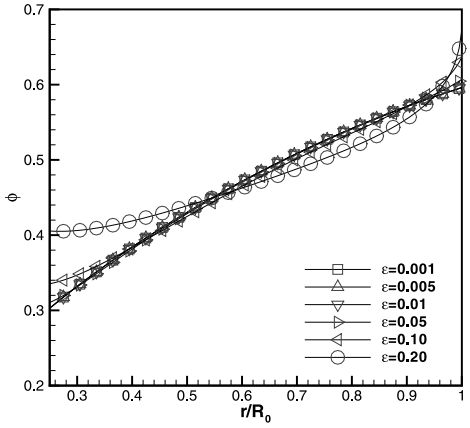

Fig. 2. The concentration profile in the Couette viscometer for $\phi_a = 0.50$ and ϵ ranging from 0.001 to 0.2.

where r has been non-dimensionalized by the tube radius R, and the velocity by the average velocity. The concentration equations for the suspension balance model and the diffusive flux models are given by, respectively,

$$\frac{\mathrm{d}}{\mathrm{d}r}\left(\sqrt{T}p(\phi)\right)+\frac{\frac{1}{2}(\sqrt{T}p(\phi))}{r}=0, \tag{66}$$

$$-K_{\mathrm{c}}a^2\phi\frac{\mathrm{d}(\dot{\gamma}\phi)}{\mathrm{d}r}-\frac{1}{2}K_{\mathrm{c}}a^2\phi\frac{\dot{\gamma}\phi}{r}-K_{\eta}a^2\dot{\gamma}\phi^2\frac{\mathrm{d}\ln\eta}{\mathrm{d}\phi}\frac{\mathrm{d}\phi}{\mathrm{d}r}=0. \tag{67}$$

The temperature equation for the suspension balance model is

$$\epsilon^2\frac{1}{r}\frac{\mathrm{d}}{\mathrm{d}r}\left(r\kappa(\phi)\frac{\mathrm{d}T}{\mathrm{d}r}\right)-\alpha(\phi)T+\eta_{\mathrm{p}}\left(\frac{\mathrm{d}u_z}{\mathrm{d}r}\right)^2=0, \tag{68}$$

where for this geometry the relative particle size is given by $\epsilon=a/R$.

The modified suspension balance model is used to predict steady-state profiles, again using $\xi=1.5$ for the pressure power index. The model predictions are compared with experimental results at bulk concentrations of $\phi_a=20\%$, 30% and 45% for relative particle size $\epsilon=0.0256$ in Fig. 3 and for relative particle size $\epsilon=0.0625$ in Fig. 4. Both the concentration and velocity

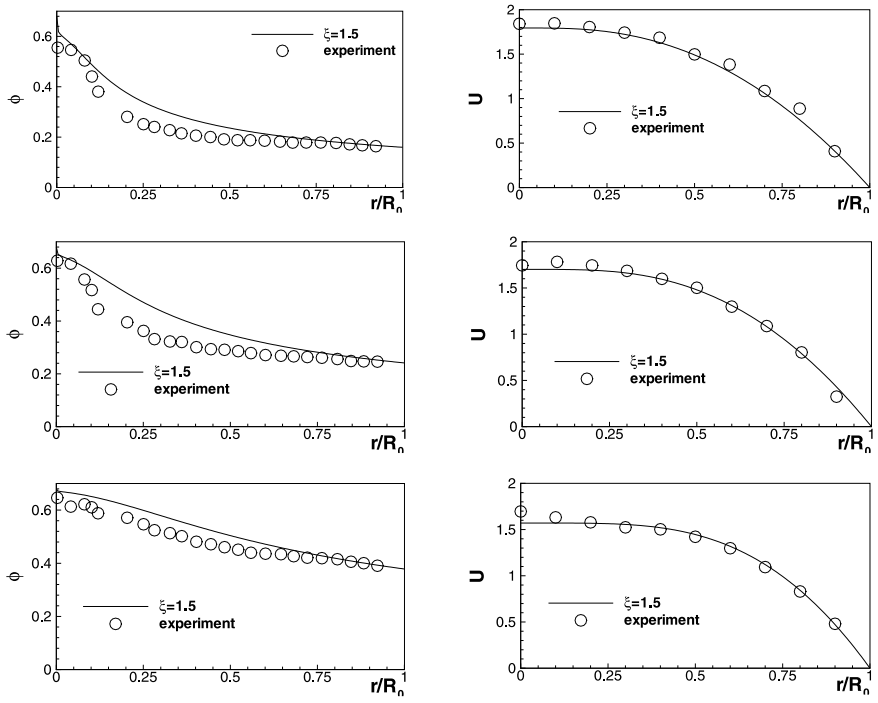

Fig. 3. Comparison of suspension balance model predicted velocity and concentration profiles for pressure-driven pipe flow with experimental data (Hampton et al., 1997) for $\epsilon=0.0256$. Top: $\phi_a=0.20$, middle: $\phi_a=0.30$, bottom: $\phi_a=0.45$.

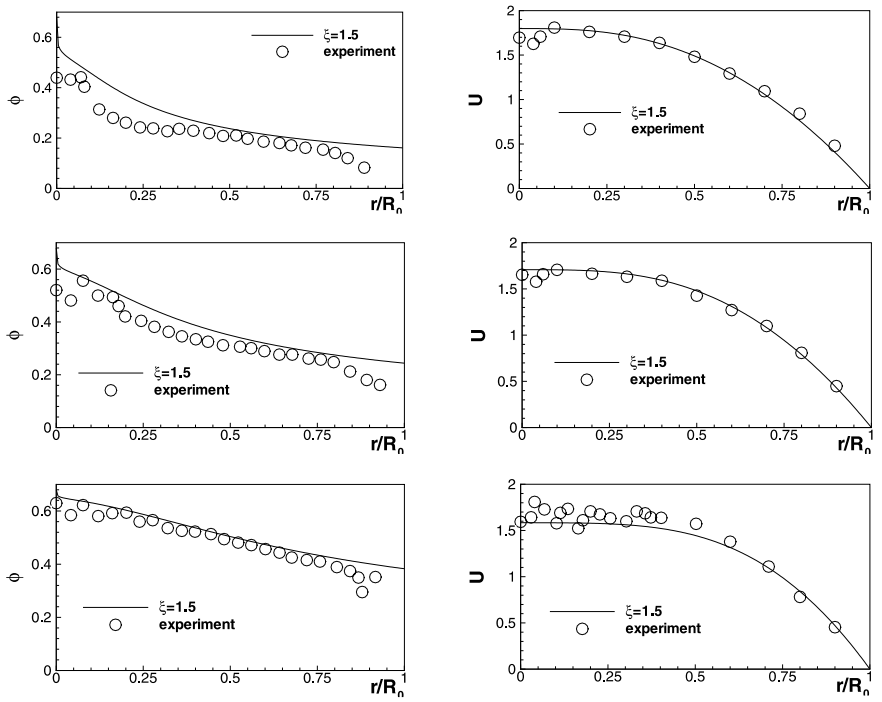

Fig. 4. Comparison of suspension balance model predicted velocity and concentration profiles for pressure-driven pipe flow with experimental data (Hampton et al., 1997) for $\epsilon = 0.0625$. Top: $\phi_a = 0.20$, middle: $\phi_a = 0.30$, bottom: $\phi_a = 0.45$.

profiles match the experimental results reasonably well. Again, the relative particle size has little influence on the steady-state profiles.

It is important to note that the introduction of anisotropy by the normal stress differences leads to migration behavior that is different from the isotropic case. This can be understood by considering the steady state, fully developed, momentum equation in the r direction in a cylindrical coordinate system

$$\frac{\partial \Pi}{\partial r} + \frac{\Pi}{2r} = 0. \tag{69}$$

Clearly, a constant particle pressure no longer satisfies the momentum equation, as was the case for the isotropic stress. This results in a different concentration profile than would be the case without normal stress differences.

The analytic solution to Eq. (67) is given by

$$\left(\frac{r}{r_{\mathrm{w}}}\right)^{1.5} = \frac{\phi_{\mathrm{w}}}{\phi}\left(\frac{\phi_{\mathrm{m}} - \phi}{\phi_{\mathrm{m}} - \phi_{\mathrm{w}}}\right)^{\xi\left(K_\eta/K_{\mathrm{c}}-1\right)}, \tag{70}$$

where r_{w} is the radius at the wall and ϕ_{w} is the concentration at the wall. This analytic solution for the modified diffusive flux model is different from that given by original model (Hampton et al., 1997) in that the power for r on the right-hand side of Eq. (70) is 1.5 instead of 1.0. As in the case

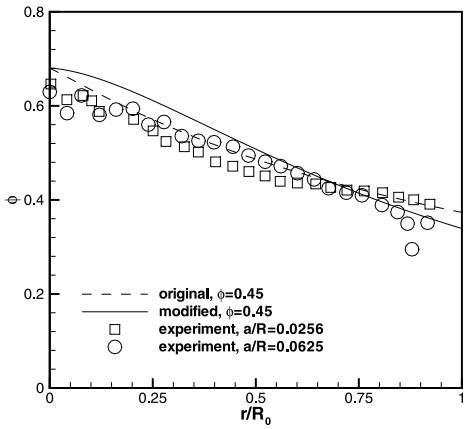

Fig. 5. Comparison of the original and modified diffusive flux model concentration profiles with experimental data (Hampton et al., 1997).

of the suspension balance model, this is a result of the second normal stress difference. The concentration profiles for the original and modified diffusive flux models are compared to experiment for a bulk concentration of $\phi_a = 45\%$ in Fig. 5. It is seen that the net effect of using the flow-aligned tensor in the diffusive flux model is to remove the cusp in the concentration profile at the centerline of the pipe.

4.3. Channel flow

For fully developed steady-state pressure-driven flow between plates (planar Poiseuille flow), the concentration profile for the modified diffusive flux model is the same as for the original model given by

$$\left(\frac{y}{y_{\mathrm{w}}}\right) = \frac{\phi_{\mathrm{w}}}{\phi}\left(\frac{\phi_{\mathrm{m}} - \phi}{\phi_{\mathrm{m}} - \phi_{\mathrm{w}}}\right)^{\xi\left(K_\eta/K_{\mathrm{c}}-1\right)}, \tag{71}$$

where y is the coordinate perpendicular to the wall and y_{w} is the value of y at the wall. The equations for modified suspension balance model are given by

$$\frac{\mathrm{d}}{\mathrm{d}y}\left(\eta_{\mathrm{r}}\frac{\mathrm{d}u}{\mathrm{d}y}\right) = -\frac{\mathrm{d}p_{\mathrm{s}}}{\mathrm{d}z}, \tag{72}$$

$$\frac{\mathrm{d}}{\mathrm{d}y}\left(\sqrt{T}p(\phi)\right) = 0, \tag{73}$$

$$\epsilon^2\frac{\mathrm{d}}{\mathrm{d}y}\left(\kappa(\phi)\frac{\mathrm{d}T}{\mathrm{d}y}\right) - \alpha(\phi)T + \eta_{\mathrm{p}}\left(\frac{\mathrm{d}u}{\mathrm{d}y}\right)^2 = 0; \tag{74}$$

in this case the relative particle size $\epsilon = a/H$, where H is the half distance between plates.

Comparisons of the model predictions with experimental results for two different relative particle sizes with bulk concentrations of $\phi_a = 30\%$ and 50% in planar Poiseuille flow is shown in

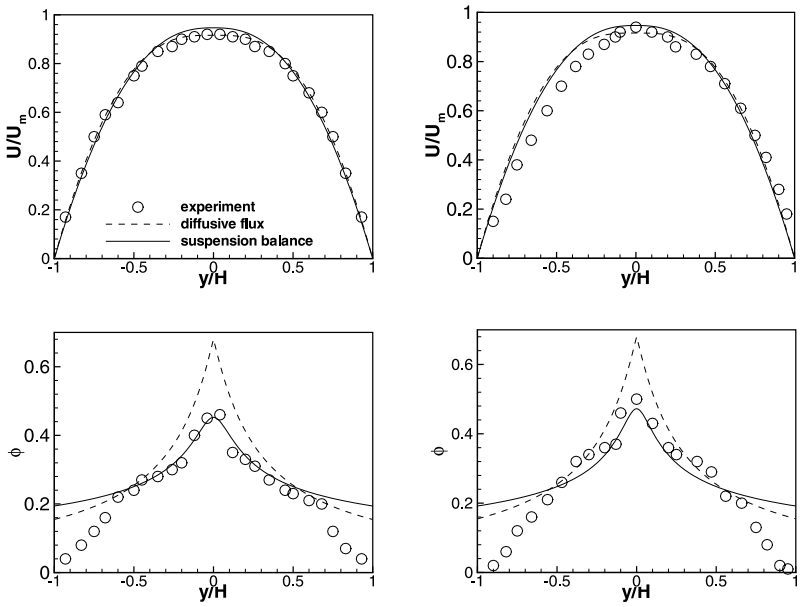

Fig. 6. Comparison of predicted velocity and concentration profiles for pressure-driven flow between plates with experimental data (Lyon and Leal, 1998) for $\phi_a = 0.30$. Left: $\epsilon = 0.0714$, right: $\epsilon = 0.0555$.

Figs. 6 and 7. The velocity is normalized with the maximum velocity, U_{m}, of a Newtonian flow with the same volume flow rate.

Qualitative comparisons with these experiments suggest that the non-locality of the suspension temperature formulation captures the basic physics near the center line. At the same bulk volume concentration, the concentration profile for larger particles has a lower peak concentration. This is a result of the finite temperature which exists at the center of the plates and is larger for the larger particle size. For the same size particles, as the bulk volume concentration increases, more particles accumulate near the midplane of the flow resulting in a larger local concentration and suspension viscosity and therefore a lower shear rate or a more blunted velocity profile. Further, as the bulk volume concentration increases, the concentration profile becomes less dependent on the relative particle size.

The diffusive flux model predicts the velocity profile well, but is less accurate predicting the concentration profile, especially near the midplane where the predicted concentration goes to maximum packing. Non-local effects could be included into the diffusive flux model by averaging the shear rate over an interaction volume.

4.4. Cone-and-plate flow

The final steady-state benchmark problem is for torsional flow in a cone-and-plate viscometer. The governing equations for the suspension balance model can be written as

$$p\sqrt{T}r^{-2} = C_{sb} \tag{75}$$

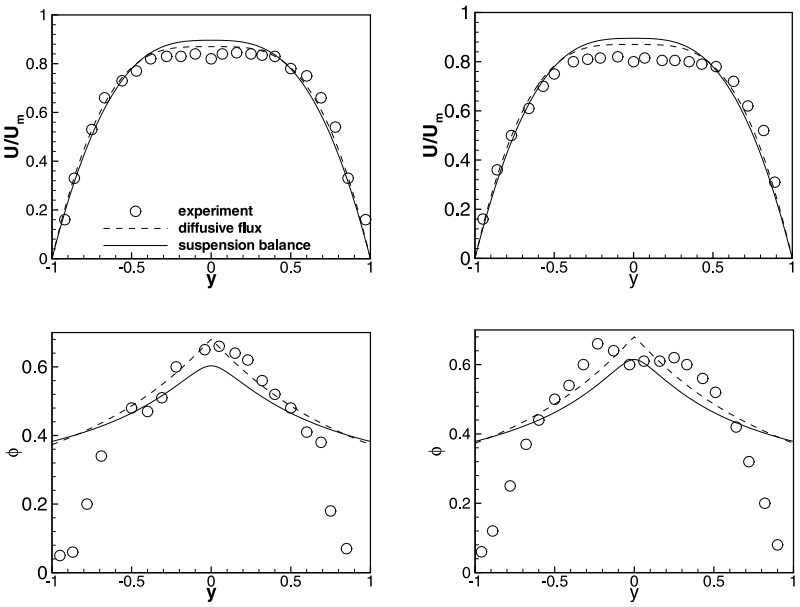

Fig. 7. Comparison of predicted velocity and concentration profiles for pressure-driven flow between plates with experimental data (Lyon and Leal, 1998) for $\phi_a = 0.50$. Left: $\epsilon = 0.0714$, right: $\epsilon = 0.0555$.

and

$$\epsilon^2 \frac{1}{r^2} \frac{\mathrm{d}}{\mathrm{d}r}\left(r^2 \kappa(\phi) \frac{\mathrm{d}T}{\mathrm{d}r}\right) - \alpha(\phi) T + \eta_{\mathrm{p}} = 0, \tag{76}$$

where C_{sb} is a constant and the relative particle size in this case is given by $\epsilon = a/R$, where R is the radius of the plate. The steady-state concentration profile for the diffusive flux model is given by

$$\frac{\phi}{r^2(\phi_{\mathrm{m}} - \phi)^{\xi(K_\eta/K_{\mathrm{c}})}} = C_{df}, \quad r > 0; \;\; \phi = 0, \;\; r = 0, \tag{77}$$

where C_{df} is a constant. The constants C_{sb} and C_{df} in Eqs. (75) and (77) are adjusted through a Newton iteration to achieve a desired bulk concentration, ϕ_a.

The steady-state concentration profiles predicted by the modified diffusive flux and the modified suspension balance models for a variety of bulk concentrations are shown in Fig. 8(a). The profiles predicted by the two models are quite similar except in the region near the cone apex. It is interesting to note that, at higher bulk concentrations, the profiles jump very quickly to 80% of their maximum values from the cone apex to a quarter length of the gap, and then increase slowly to their maximum values at the outer edge of the cone-and-plate device.

Because of physical difficulties, cone-and-plate viscometers cannot be used to measure properties of suspensions of finite-sized particles, and the cone is truncated near the apex. To compare these model results to experimental results in truncated cone-and-plate geometries, the concentration profiles are assumed to be constant in the small parallel plate truncation region. Particles outside this region experience an outward migration. Comparisons between the experimental

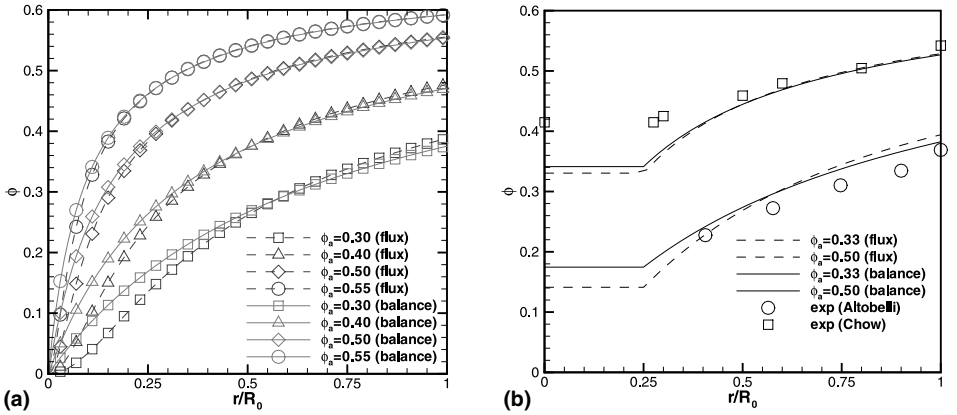

Fig. 8. (a) Predicted concentration profiles in a cone-and-plate geometry for $\phi_a = 30\%$, 40%, 50% and 55%. (b) Comparison of predicted concentration profiles with experimental data in a truncated cone-and-plate geometry for $\phi_a = 33\%$ and 50%. Squares (50%) are from Chow et al. (1995), circles (33%) are from Mondy and Altobelli (1999).

results and the model predictions are shown in Fig. 8(b). The model predictions show reasonably good agreement with experimental data for both low and high bulk volume fractions.

5. Transient flows

Transient calculations of circular Couette flow, eccentric journal bearing flow, and piston-driven flow are discussed in this section. The diffusive flux calculations for circular Couette flow and eccentric journal bearing flow are the same for the original and modified models because $\lambda_1 = \lambda_2$ and there is no out-of-plane migration.

5.1. FD and FEM codes

For the Couette flow, a one-dimensional finite difference scheme was used, while a Galerkin finite element method (FEM) was used for the fully two-dimensional calculations. A brief outline of the two-dimensional FEM formulation used to solve the governing equations for the suspension balance model is given below.

First, the governing system of equations is recast in dimensionless form by choosing characteristic length, velocity, pressure, temperature, and time scales. For example, for Couette flow the length scale is chosen to be the distance between the cylinders H, the velocity scale is chosen to the velocity of the rotating cylinder $U = \Omega R$, the pressure scale is chosen to be $\eta_s U/H$, the temperature scale is chosen to be a^2U^2/H^2, and the time scale is chosen to be H/U. The dimensionless form of the governing equations at low Reynolds number is therefore

$$\nabla \cdot \langle \mathbf{u} \rangle = 0, \tag{78}$$

$$-\nabla \langle p \rangle_f - \nabla \cdot \Pi \mathbf{Z} + \nabla \cdot 2\eta_r(\phi)\langle \mathbf{e} \rangle = 0, \tag{79}$$

$$\epsilon^2 \nabla \cdot \kappa(\phi)\nabla T - \alpha(\phi)T - \Pi \mathbf{Z} : \langle \mathbf{e} \rangle + 2\eta_p \langle \mathbf{e} \rangle : \langle \mathbf{e} \rangle = 0, \tag{80}$$

$$\frac{\partial \phi}{\partial t} + \langle \mathbf{u} \rangle \cdot \nabla \phi = \epsilon^2 (\nabla \cdot M \phi \nabla \cdot \Pi \mathbf{Z} - \nabla \cdot f \phi \nabla \cdot 2\eta_{\mathrm{p}} \langle \mathbf{e} \rangle), \tag{81}$$

where all variables are now dimensionless.

The interpolation functions for velocity components, concentration, and temperature are chosen to be biquadratic, while those for pressure are chosen to be bilinear. The method of lines is used to discretize time using backwards Euler differencing. For each time step, the following iteration is used:

1. Eqs. (78) and (79) are solved simultaneously to determine updated values for the velocity components and pressure field.
2. Eq. (80) is solved to determine updated values for the temperature field.
3. Eq. (81) is solved to determine updated values for the concentration field.
4. Check for convergence. If the solution is converged, advance the time step. If the solution is not converged, go to Step 1.

In Eqs. (79) and (80), values for ϕ at the first iteration step are taken from the previous time step and subsequently from the previous iteration step.

There are second-order derivatives of velocity in the concentration equation which can cause numerical difficulties. A smoothing algorithm is employed that averages values determined from adjacent elements at a common node. The variation in the viscosity as the concentration approaches maximum packing makes the differential system stiff for highly loaded systems. The variation in the viscosity between adjacent nodes can be as large as a few orders of magnitude. To avoid convergence problems, an elemental smoothing algorithm and under-relaxation is employed in the calculation of the viscosity based on the Krieger formula (Eq. (15)).

Since the flow-aligned tensor $\mathbf{Z}$ is defined in terms of the modified shear coordinates described above and the FEM code uses Cartesian coordinates, a transformation tensor must be determined from the calculated velocity field after each iteration and at each grid point. The FEM code was first benchmarked by considering the transient circular Couette flow described in the following section. Because the FEM code is two-dimensional, the CPU time was significantly larger than the one-dimensional Crank–Nicholson method when used to predict the circular Couette flow.

5.2. Circular Couette flow

Transient concentration and velocity profiles in Couette flows have been obtained recently by Tetlow et al. (1998), and previously, by Abbott et al. (1991). It is therefore appropriate to use these data to calibrate the values of the coefficient that governs the rate of profile evolution for the suspension balance model, namely k_ϕ (Eq. (38)). For circular Couette flow, the governing equations for the suspension balance model reduce to

$$\epsilon^2 \mathrm{Re} \frac{\mathrm{d}u_\theta}{\mathrm{d}t} = \frac{1}{r^2} \frac{\mathrm{d}}{\mathrm{d}r} \left[r^3 \eta_{\mathrm{r}} \frac{\mathrm{d}}{\mathrm{d}r} \left(\frac{u_\theta}{r} \right) \right], \tag{82}$$

$$\epsilon^2 \frac{1}{r} \frac{\mathrm{d}}{\mathrm{d}r} \left[r \kappa(\phi) \frac{\mathrm{d}T}{\mathrm{d}r} \right] - \alpha(\phi) T + \eta_{\mathrm{p}} \left[r \frac{\mathrm{d}}{\mathrm{d}r} \left(\frac{u_\theta}{r} \right) \right]^2 = 0, \tag{83}$$

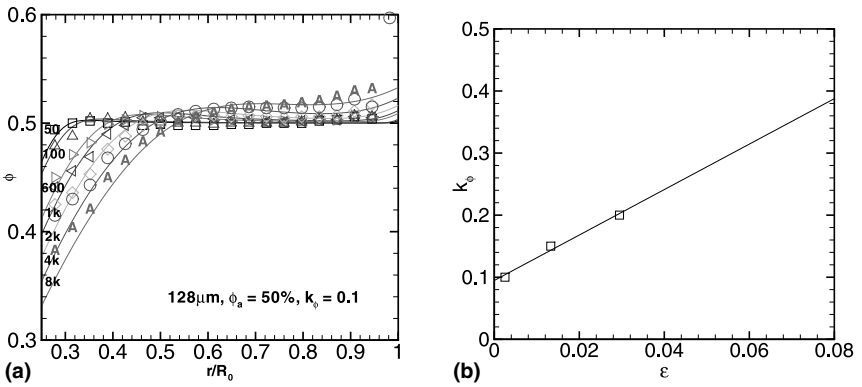

Fig. 9. (a) Comparison of predicted transient profiles for $\epsilon = 0.02836$, $k_\phi = 0.1$ and $\phi_a = 0.5$ with the corresponding experimental data; (b) optimal k_ϕ as a function of ϵ.

$$\frac{\mathrm{d}\phi}{\mathrm{d}t} = \frac{1}{r}\frac{\mathrm{d}}{\mathrm{d}r}\left[rf(\phi)\frac{\mathrm{d}}{\mathrm{d}r}\left(p(\phi)\sqrt{T}\right)\right]. \tag{84}$$

A Crank–Nicholson method is used to solve this set of equations for the one-dimensional flow field.

The parameter k_ϕ is estimated by comparing the current model results to experimental results described by Phillips et al. (1992) and Tetlow et al. (1998). To best fit the experimental data, the parameter k_ϕ is chosen as a function of ϵ. Fig. 9(a) shows the transient concentration profiles that best fit the experimental data for the case where $\epsilon = 0.02836$, with the corresponding values of k_ϕ in Fig. 9(b).

Although the reason why k_ϕ is a function of ϵ is unclear, the likely cause is that some physics is missing from the model. Note also that Tetlow et al. (1998) found that the experimental rates of profile evolution do not scale with ϵ^2, as predicted by both suspension balance and diffusive flux models, but with $\epsilon^{2.7}$. Hampton et al. (1997), on the other hand, found the rates of profile evolution to vary with $\epsilon^{0.4}$ at low ϕ, to $\epsilon^{1.8}$ at high ϕ. It is possible that for the relatively large values of ϵ used in the experiments, finite particle size effects are present. For example, a stagnant wall layer of particles at solid boundaries may reduce the effective device dimensions. Experiments are currently being undertaken to verify this hypothesis. For the diffusive flux model, the values of K_c and K_η available in the literature are used here.

5.3. Eccentric journal bearing flow

Suspension flows in eccentric journal bearing geometries have been studied by Phan-thien et al. (1995) and Subia et al. (1998). The eccentricity is defined as the offset of the inner cylinder from the outer cylinder divided by the difference of the outer and inner radii. A comparison of the results generated using the modified diffusive flux, the modified suspension balance model and experiment for an eccentricity of 1/2 is shown in Fig. 10 for a bulk concentration of $\phi_a = 0.50$.

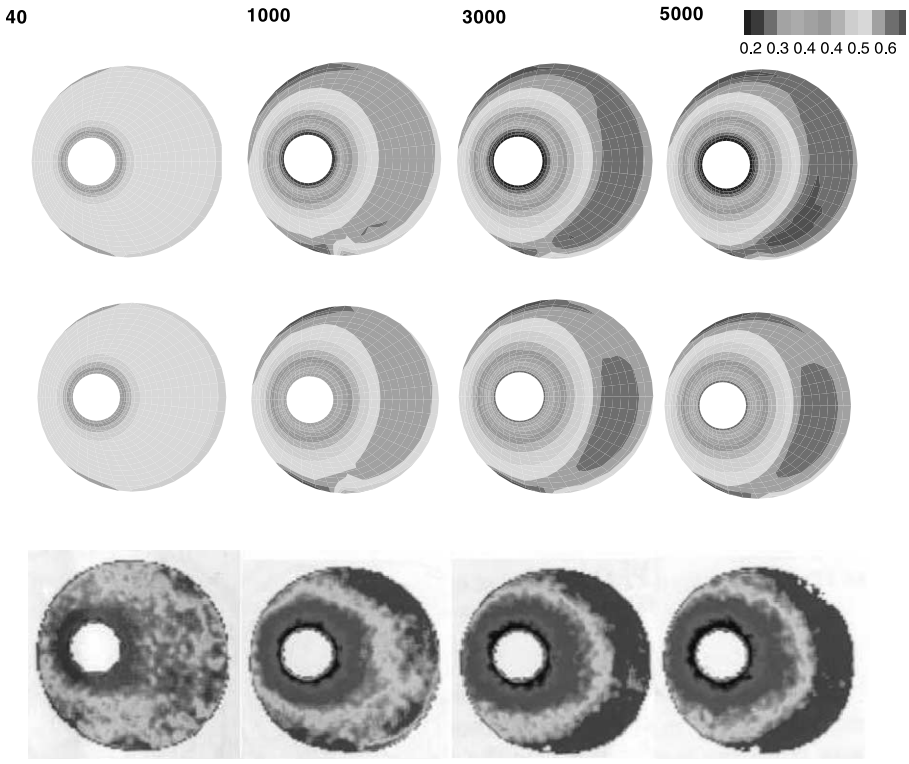

Fig. 10. Transient concentration contours in an eccentric journal bearing flow ($e/c = 1/2$) for a bulk volume fraction $\phi_a = 0.50$ and relative particle size $\epsilon = 0.02836$. The top, middle and bottom rows of figures are results from the diffusive flux model, the suspension balance model, and experiment, respectively. The number above each column of figures represents the number of counterclockwise turns of the inner cylinder.

The current calculation exhibits similar qualitative features as predicted by the original diffusive flux model (Subia et al., 1998) and is consistent with the experimental data. The particles generally migrate away from the rotating inner cylinder into three discrete regions: the compression flow area above rotating inner cylinder, the expansion flow area below the inner cylinder, and the wide gap recirculation region. Unlike circular Couette flow, the maximum solid-phase concentration is not uniform at the outer wall; in the wide-gap region the maximum concentration occurs in the interior of the recirculation zone.

There is an interesting feature in the concentration profile that occurs between the expansion flow area and the wide gap recirculation region near the bottom of the outer cylinder. There is a region of high concentration at the bottom of the expansion region followed by a relatively sharp concentration gradient leading to low concentration at the bottom of the recirculation region. This feature can be seen at 1000 and 2000 revolutions in the experimental data but then seems to disappear. The numerical simulations show this feature to be much more persistent. The high concentration region can be explained by particles piling up coming out of the expansion region and running into the dividing streamline of the recirculation region. It is conjectured that the low concentration region is caused by wall effects which cause particle velocities near the wall to lag fluid velocities.

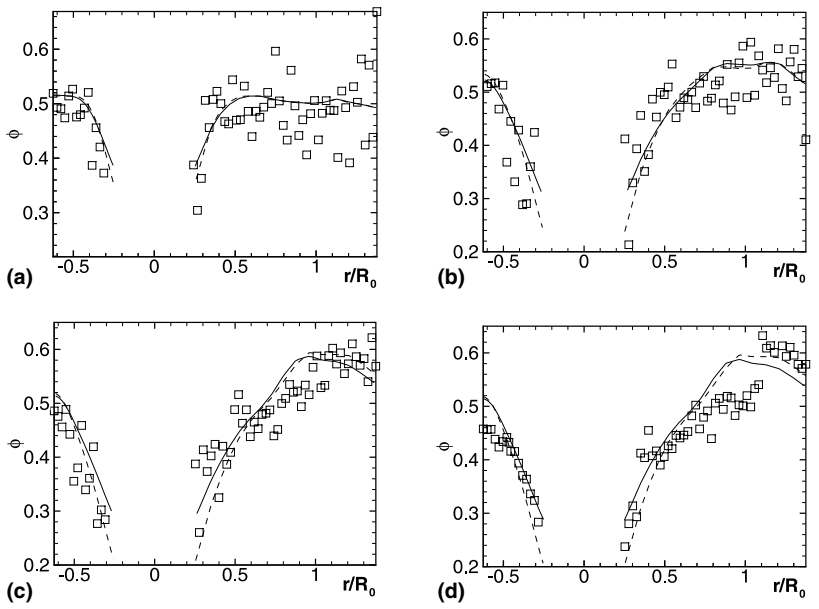

Fig. 11. Comparison between computed concentration and experimental data along the horizontal midplane of the eccentric journal bearing for a bulk volume fraction $\phi_a = 0.50$ and relative particle size $\epsilon = 0.02836$. Squares are experimental data, solid lines are suspension balance model predictions and dashed lines are diffusive flux model predictions.

A more quantitative comparison of the experimental data with the modified suspension balance model and the modified diffusive flux model, along the midplane of the eccentric journal bearing, is shown in Fig. 11.

Good agreement is seen between the models and experimental results. The scatter in the experimental data compared to similar results for circular Couette flow is caused by the fact that no polar averaging can be performed in the non-axisymmetric geometry.

5.4. Piston driven flow

In this flow geometry, the second normal stress difference plays a significant role in the suspension behavior. Comparison with isotropic simulations (Subia et al., 1998) will show the effect of the second normal stress difference on the evolution of the concentration profiles. The experimental apparatus and setup have already been explained in detail by Subia et al. (1998), and the description will not be repeated here. For the numerical simulations, an identical set of boundary conditions is adopted, namely stationary pistons and moving walls.

Fig. 12 shows a comparison between concentration contours calculated with the diffusive flux model and with the suspension balance model, for $\epsilon = 0.0625$. The value of k_ϕ for this particle size is obtained by extrapolation using Fig. 9(b). The two models give similar results, the only noticeable difference being the stronger particle depletion at the trailing piston face obtained with the diffusive flux model. Comparison of the modified diffusive flux model results, where the constitutive equation is modified to include normal stress differences, with the simulations results pre-

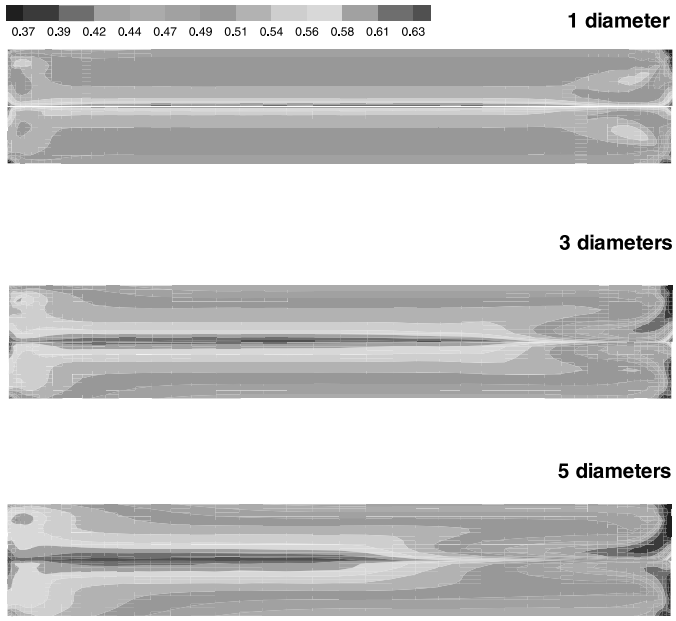

Fig. 12. Predicted contours of concentration adjacent to the aft piston (right) and to forward piston (left) after piston travel 1 diameter, 3 diameters and 5 diameters by the suspension balance model (lower) and the diffusive flux model (upper) for $\epsilon = 0.0625$. The walls move from left to right.

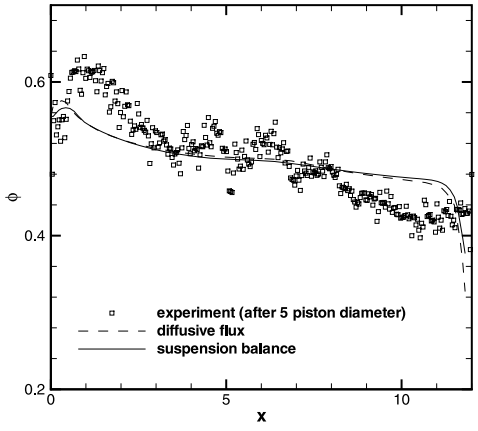

Fig. 13. Comparison between model predictions and experimental data on area-average concentration along piston axis for $\epsilon = 0.0625$. Dashed lines are the diffusive flux results and solid lines are the suspension balance results, and the squares are experimental data.

sented by Subia et al. (1998), indicates that the effect of the normal stress differences is to reduce the rate of particle migration for this geometry.

Fig. 13 shows a comparison between model predictions using the modified diffusive flux model, the modified suspension balance model and experimental data for area averaged particle volume fraction along the piston axis for $\epsilon = 0.0625$.

Both models predict a slower migration rate than experiment data, especially at the piston faces, although the models are in good agreement with each other. The reason for this discrepancy is unclear and may point to a feature that is missing in both models as currently formulated, namely the effects of particle-phase compressibility on the transient response.

6. Summary of numerical implementation

In this section, the implementation of the model for a generic flow field (such as might be found in the course of the FEM simulation of an arbitrary flow) is described, for the suspension balance model and for the diffusive flux model. In both cases, the initial particle concentration (ϕ) field is required, as well as the boundary conditions.

First, consider the suspension balance model. Because the initial ϕ field is known, the velocity field can be found using the governing equations (1) and (2), together with the constitutive equations for the suspension and the particle phase (4) and (12). The particle relative viscosity η_p particle pressure Π in Eq. (12) can be obtained using the ancillary relations (14), (15), (36) and (38). Determination of the particle pressure requires the suspension temperature, T, which can be obtained using the mechanical energy balance, Eq. (39), with ancillary relations (42), (46) and (47). The solution of the coupled energy and momentum equations can be carried out using standard methods, and needs no further elaboration.

The only difficulty here is that the flow-aligned directions $\boldsymbol{\delta}_1$, $\boldsymbol{\delta}_2$ and $\boldsymbol{\delta}_3$ are not known a priori, except in simple flows such as the ones considered here. In the general case, when starting a transient simulation, the flow can be solved by initially assuming an isotropic $\mathbf{Z}$ to obtain an estimate of the flow-aligned directions, and subsequently correcting for anisotropy by iteration. For subsequent steps, the flow-aligned directions from the previous steps can be used as an initial estimate for the current step.

After solution of the flow kinematics, it is necessary to update the particle concentration field. This can be done using the particle conservation equation, Eq. (7), and the particle flux equation, Eq. (8). The drag force in Eq. (8) is given by Eq. (10), while the mobility is obtained using Eqs. (44) and (45). The coefficients that appear in the aforementioned equations are summarized in Table 1.

Next, consider the modified diffusive flux model. As in the case of the suspension balance model, the kinematics of the flow are solved using the governing equations (1) and (2) and the constitutive equation for the stress, Eq. (59). As with the suspension balance model, the flow-aligned directions

Table 1
Coefficients used in the suspension balance model calculations

ϕ_m	0.68
k_α	0.19
k_κ	0.17
k_ϕ	$0.095 + 3.65\epsilon$
ξ	1.5
λ_1	1.2
λ_2	1.2
λ_3	0.6

Table 2
Coefficients used in the diffusive flux model calculations

K_c	0.41
K_η	0.62
λ_1	1.2
λ_2	1.2
λ_3	0.6

are generally unknown a priori, but can be found by iteration. Note that, because of the absence of an energy equation, the kinematic solution is considerably simpler with the modified diffusive flux model. The particle concentration field can then be updated using the particle phase conservation equation, Eq. (52), where the particle flux terms are provided by Eqs. (53) and (54). The coefficients used in the modified diffusive flux model calculations are as shown in Table 2.

7. Discussion and conclusions

Two major classes of models exist for the simulation of the flow of heavily concentrated suspensions: the suspension balance model and the diffusive flux model. Both models suffered from shortcomings when compared to a particular set of experimental results. To correct these shortcomings, a flow-aligned directional tensor is introduced into the suspension balance model and, by analogy, into the diffusive flux model. The flow-aligned tensor accommodates the non-isotropic nature of diffusion and migration processes in suspension flows at low Reynolds number. Because a flow-aligned tensor can be found for arbitrary flow conditions, this formulation is well-suited for general application in the simulation of complex flows.

The approach used to derive the model is similar to that taken by Morris and Boulay (1999). The normal stress difference coefficients are inferred by noting that the radial migration in torsional flow between parallel plates is either zero or too small to detect, and with the well founded assumption that there is no azimuthal migration in a cone-and-plate experiment. The results obtained by Morris and Boulay are very similar, even though they used experimental results from a Couette experiment instead of the cone-and-plate assumption adopted here.

As well as corroborating the work of Morris and Boulay, this study provides additional insight into the non-isotropic behavior of suspension flows. First, it is shown that normal stress differences not only affect curvilinear flows, but also flows in which the streamlines are straight lines; here the effects are in terms of migration rate and concentration profiles in geometries such as Poiseuille flow. Second, it is shown that the diffusive flux model can describe anisotropic particle migration, provided that the flux terms are appropriately modified and that the fluid rheology is consistent with the modified diffusive flux. Third, both models have been implemented in a finite element analysis code, allowing the simulation of fully two-dimensional transient flows.

The suspension balance model is more rigorous since migration follows directly from the constitutive behavior of the suspension. In the diffusive flux model, on the other hand, the diffusion is decoupled from the rheology of the suspension, and care must be taken to maintain consistency between the two. However, the diffusive flux model has an advantage in terms of

robustness and speed, and therefore may be more attractive for the purposes of large numerical calculations. Because the results of the two models do not differ significantly, the diffusive flux model can be used with confidence to simulate such flows.

Comparisons of two-dimensional flow predictions with the corresponding experimental results show good correlation. In the case of the eccentric journal bearing flow, the normal stress differences had no effect, because isotropic conditions exist in the plane of flow. In this case, quantitative agreement is found for both rate and particle distributions. The more interesting comparison, the piston driven flow, shows good qualitative agreement for both the suspension balance and diffusive flux models with the experimentally determined particle concentration profiles. The rate of migration, however, was somewhat underpredicted by both models. The reasons for this discrepancy are not clear, and more experiments are required to obtain more conclusive data.

Finally, Stokesian Dynamics simulations predict a small negative first normal stress difference, while the constraint that there should be no migration in a torsional flow between parallel plates results in a zero normal stress difference. At small values of N_1, both the suspension balance and the diffusive flux models would predict very small radial particle fluxes for the parallel plate geometry, which would probably not be detectable in the type of experiments commonly used to measure suspension properties.

Acknowledgements

This work was partially supported by the US Department of Energy under Contract DE-AC04-94AL85000 at Sandia National Laboratories. Sandia is a multiprogram laboratory operated by Sandia Corporation, a Lockheed Martin Company, for the United States Department of Energy. Partial support was also provided by Division of Material Science and Engineering, Office of Basic Energy Sciences, US DOE, and Division of Chemical Sciences, Geosciences, and Biosciences, Office of Basic Energy Sciences, U. S. DOE. Partial support was also provided by a ''rand Challenge'' award sponsored by the Mathematical, Information, and Computational Sciences Division, Office of Computational and Technology Research, Office of Energy Research, US DOE.

References

Abbott, J.R., Tetlow, N., Graham, A.L., Altobelli, S.A., Fukushima, E., Mondy, L.A., Stephens, T.S., 1991. Experimental observation of particle migration in concentrated suspensions: Couette flow. J. Rheol. 35, 773–795.

Batchelor, G.K., 1970. The stress in a suspension of force-free particles. J. Fluid Mech. 41, 545–570.

Bird, R.B., Armstrong, R.C., Hassager, O., 1977. Dynamics of Polymeric Liquids. Wiley, New York.

Brady, J.F., 1993. The rheological behavior of concentrated colloidal dispersion. J. Chem. Phys. 99, 567–581.

Brady, J.F., Bossis, G., 1985. The rheology of concentrated suspensions of spheres in simple shear flow by numerical simulation. J. Fluid Mech. 155, 105–129.

Brady, J.F., Bossis, G., 1988. Stokesian dynamics. Ann. Rev. Fluid Mech. 20, 111–157.

Brady, J.F., Morris, J.F., 1997. Microstructure of strongly sheared suspensions and its impact on rheology and diffusion. J. Fluid Mech. 348, 103–139.

Brady, J.F., Phillips, R.J., Lester, J.C., Bossis, G., 1988. Dynamic simulation of hydrodynamically interacting suspensions. J. Fluid Mech. 195, 257–280.

Buyevich, I.A., 1995. Particle distribution in suspension shear flow. Chem. Eng. Sci. 51 (4), 635–647.
Buyevich, Y.A., Kapbsov, S.K., 1999. Segregation of a fine suspension in channel flow. J. Non-Newtonian Fluid Mech. 86, 157–184.
Chapman, B.K., 1990. Shear induced migration phenomena in concentrated suspensions. Ph.D. Thesis, University of Notre Dame.
Chen, D., Doi, M., 1995. Simulation of aggregating colloids in shear flow. J. Chem. Phys. 91, 2656–2663.
Chow, A.W., Iwamiya, J.H., Sinton, S.W., Leighton Jr., D.T., 1995. Particle migration of non-Brownian, concentrated suspensions in a truncated cone-and-plate. Poster at Society of Rheology Meeting, Sacramento, CA, unpublished.
Chow, A.W., Sinton, S.W., Iwamiya, J.H., 1994. Shear-induced particle migration in Couette and parallel-plate viscometers: NMR imaging and stress measurements. Phys. Fluids 6, 2561–2575.
Foss, D.R., Brady, J.F., 1999. Self-diffusion in sheared suspensions by dynamic simulation. J. Fluid Mech. 401, 243–274.
Hampton, R.E., Mammoli, A.A., Graham, A.L., Altobelli, S.A., 1997. Migration of particles undergoing pressure-driven flow in a circular conduit. J. Rheol. 41 (3), 621–639.
Ingber, M.S., Womble, D.E., Mondy, L.A., 1994. A parallel boundary elitent formulation for determining effective properties of heterogeneous media. J. Numer. Meth. Eng. 37, 3905–3919.
Jenkins, J.T., McTigue, D.F., 1990. Transport process in concentrated suspensions: the role of particles fluctuations. In: Joseph, D.D., Schaeffer, D.G. (Eds.), Two Phase Flows and Waves Pages. Springer, New York, pp. 70–79.
Kapoor, B., Acrivos, A., 1995. Sedimentation and sediment flow in settling tanks with inclined walls. J. Fluid Mech. 290, 39–66.
Krishnan, G.P., Beimfohr, S., Leighton Jr., D.T., 1996. Shear-induced radial segregation in bidisperse suspensions. J. Fluid Mech. 321, 371–393.
Leighton Jr., D.T., Acrivos, A., 1987a. Measurement of shear-induced self-diffusion in concentrated suspensions of spheres. J. Fluid Mech. 177, 109–131.
Leighton Jr., D.T., Acrivos, A., 1987b. The shear-induced migration of particles in concentrated suspensions. J. Fluid Mech. 181, 415–439.
Lyon, M.K., Leal, L.G., 1998. An experimental study of the motion of concentrated suspensions in two-dimensional channel flow. i. monodisperse systits. J. Fluid Mech. 363, 25–56.
Mondy, L.A., Altobelli, S.A., 1999, personal communication.
Morris, J.F., Boulay, F., 1999. Curvilinear flows of noncolloidal suspensions: the role of normal stresses. J. Rheol. 43, 1213–1237.
Morris, J.F., Brady, J.F., 1998. Pressure-driven flow of a suspension: buoyancy effects. Int. J. Multiphase Flow 24, 105–130.
Nott, P.R., Brady, J.F., 1994. Pressure-driven flow of suspensions: simulation and theory. J. Fluid Mech. 275, 157–199.
Phan-thien, N., Graham, A.L., Altobelli, S.A., Abbott, J.R., Mondy, L.A., 1995. Hydrodynamic particle migration in a concentrated suspension undergoing flow between rotating eccentric cylinders. Ind. Eng. Chem. Res. 34, 3187–3194.
Phan-Thien, N., Kim, S., 1994. Microstructures in Elastic Media: Principles and Computational Methods. Oxford, New York.
Phillips, R.J., Armstrong, R.C., Brown, R.A., Graham, A.L., Abbott, J.R., 1992. A constitutive equation for concentrated suspension that accounts for shear-induced particle migration. Phys. Fluids A 4, 30–40.
Phung, T.N., Brady, J.F., Bossis, G., 1996. Stokesian dynamics simulation of brownian suspensions. J. Fluid Mech. 313, 181–207.
Sami, S., 1996. Stokesian dynamics simulations of brownian suspensions in extensional flow. Master's Thesis, California Institute of Technology.
Subia, S.R., Ingber, M.S., Mondy, L.A., Altobelli, S.A., Graham, A.L., 1998. Modeling of concentrated suspensions using a continuum constitutive equation. J. Fluid Mech. 373, 193–219.
Tetlow, N., Graham, A.L., Ingber, M.S., Subia, S.R., Mondy, L.A., 1998. Particle migration in a Couette apparatus: experiment and modeling. J. Rheol. 42, 307–327.
Yurkovetsky, Y., Brady, J.F., 1996. Statistical mechanics of bubbly liquids. Phys. Fluids 8, 881–895.
Zarraga, I.E., Hill, D.A., Leighton Jr., D.T., 2000. The characterization of the total stress of concentrated suspensions of noncolloidal spheres in Newtonian fluids. J. Rheol. 44, 185–220.